44p.

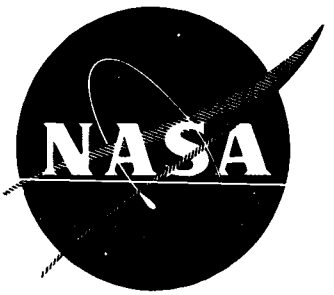

MEASURED AND CALCULATED NUCLEAR RADIATION DISTRIBUTIONS IN LIQUID HYDROGEN

by

W. A. Hehs and G. E. Miller

27 Mar. 1964

44p refs

prepared for

NATIONAL AERONAUTICS AND SPACE ADMINISTRATION

(NASA Contract NAS 3-3324)

NUCLEAR AEROSPACE RESEARCH FACILITY

operated by
General Dynamics / Fort Worth, Tex.

NASA CR-54003

FZK-182

TOPICAL REPORT

MEASURED AND CALCULATED NUCLEAR RADIATION DISTRIBUTIONS IN LIQUID HYDROGEN

by

W. A. Hehs and G. E. Miller

prepared for

NATIONAL AERONAUTICS AND SPACE ADMINISTRATION

27 MARCH 1964

Contract NAS 3-3324

Technical Management
NASA-Lewis Research Center
Advanced Development and Evaluation Division
Cleveland, Ohio
D. J. Connolley

NUCLEAR AEROSPACE RESEARCH FACILITY

operated by
General Dynamics / Fort Worth

FOREWORD

The purpose of this topical report is to make the nuclear-radiation data available for distribution before publication of the final report of the contract and, thus, to allow its use at an earlier date. The work described in this report was supported by the National Aeronautics and Space Administration and was directed by Lewis Research Center under Contract NAS 3-3324. The Project Engineers for NASA and General Dynamics/Fort Worth were D. J. Connolley and W. A. Hehs, respectively.

SUMMARY

18350 A

The nuclear radiation measurements and calculations obtained from a series of experiments designed to investigate the effects of nuclear heating in liquid hydrogen are reported. The experimental arrangement simulated the radiation source and liquid-hydrogen propellant-tank geometry of a typical nuclear rocket system. The operating capacity of the tank was approximately 125 gallons.

Nuclear radiation measurements were made in and around the liquid-hydrogen tank with the tank both empty and full of hydrogen. The radiation detectors and techniques used in making these measurements are described, and the measurements are compared with calculated nuclear radiation intensities. The calculations include secondary-gamma-ray production in the liquid hydrogen as well as in other surrounding materials. Assumptions and methods utilized in performing these calculations are discussed. The measured and calculated radiation intensities are, in general, in quite good agreement. Author

TABLE OF CONTENTS

LIST OF FIGURES

LIST OF TABLES

1. INTRODUCTION

Various computer programs have been employed to calculate the nuclear radiation attenuation and energy deposition in the liquid-hydrogen propellant of nuclear rocket systems. To date, only limited experimental data have been available for comparison with results of the computer programs. Consequently, it has been difficult to verify methods and results of the programs and to assign a degree of reliability or accuracy to the calculations. This report presents a considerable amount of experimental nuclear data that were obtained during a series of experiments designed to investigate the effects of heating due to nuclear energy deposition in liquid hydrogen. Because these nuclear data were obtained in a geometry simulating the radiation source and liquid-hydrogen propellant tank of a typical nuclear system, they can readily serve as a basis for checking and comparing the results of the various computer programs. The experimental geometry is described in sufficient detail to allow other investigators to duplicate the geometry in checking computer codes and to permit direct comparison of calculated data with the measured data presented in this report.

The nuclear data presented here are only some of the results from the experiments performed at the Nuclear Aerospace Research Facility (NARF) and sponsored by the National Aeronautics and Space Administration's Lewis Research Center. The purpose of this report is to allow early distribution and use of the nuclear data. Further analysis and conclusions regarding these data will be presented in a comprehensive final report.

2. EXPERIMENTAL ARRANGEMENT AND PROCEDURES

2.1 Experimental Geometry

The experimental arrangement was designed to simulate the radiation source and the liquid-hydrogen propellant-tank geometry of a typical nuclear rocket system. A sketch of the experimental setup is shown in Figure 1. The Aerospace Systems Test Reactor (ASTR) was utilized as the source of nuclear radiation, and a 125-gal liquid-hydrogen tank was used as a scaled-down propellant tank. As shown in Figure 1, the liner tank provided a space in which the LH_2 tank was positioned immediately above the reactor pressure vessel. The water tank and steel sheets above the liner tank and LH_2 tank provided shielding to reduce the radiation leakage to the surrounding area to tolerable levels.

Greater detail of the reactor—hydrogen-tank geometry is given in Figures 2 and 3. The LH_2 tank was of the typical cylindrical shape with a conical bottom. The diameter of the cylinder was 32 in. and the half-angle of the conical bottom was 45°. The stainless-steel walls of the tank varied slightly in thickness from one section to another, as indicated in Figure 2.

The ASTR is a water-moderated reactor, with MTR-type fuel elements contained in a stainless-steel pressure vessel. A void section was placed inside the pressure vessel to increase the neutron leakage from the reactor in the area under the LH_2 tank.

During the experiment, the reactor was raised to either of the two positions shown in Figure 3. In the position referred to as Configuration 1, the reactor pressure vessel was immediately

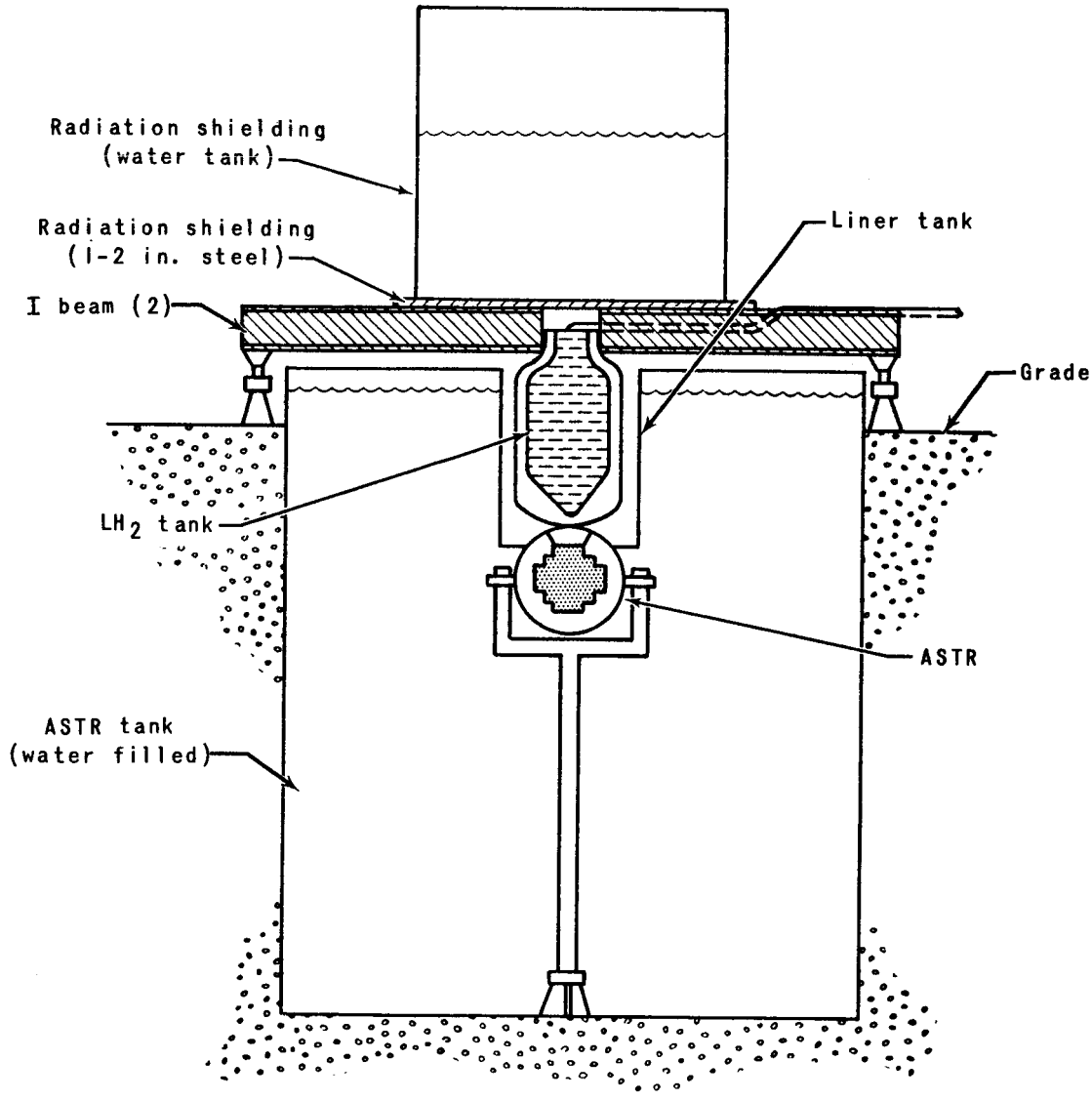

Figure 1 Experimental Setup

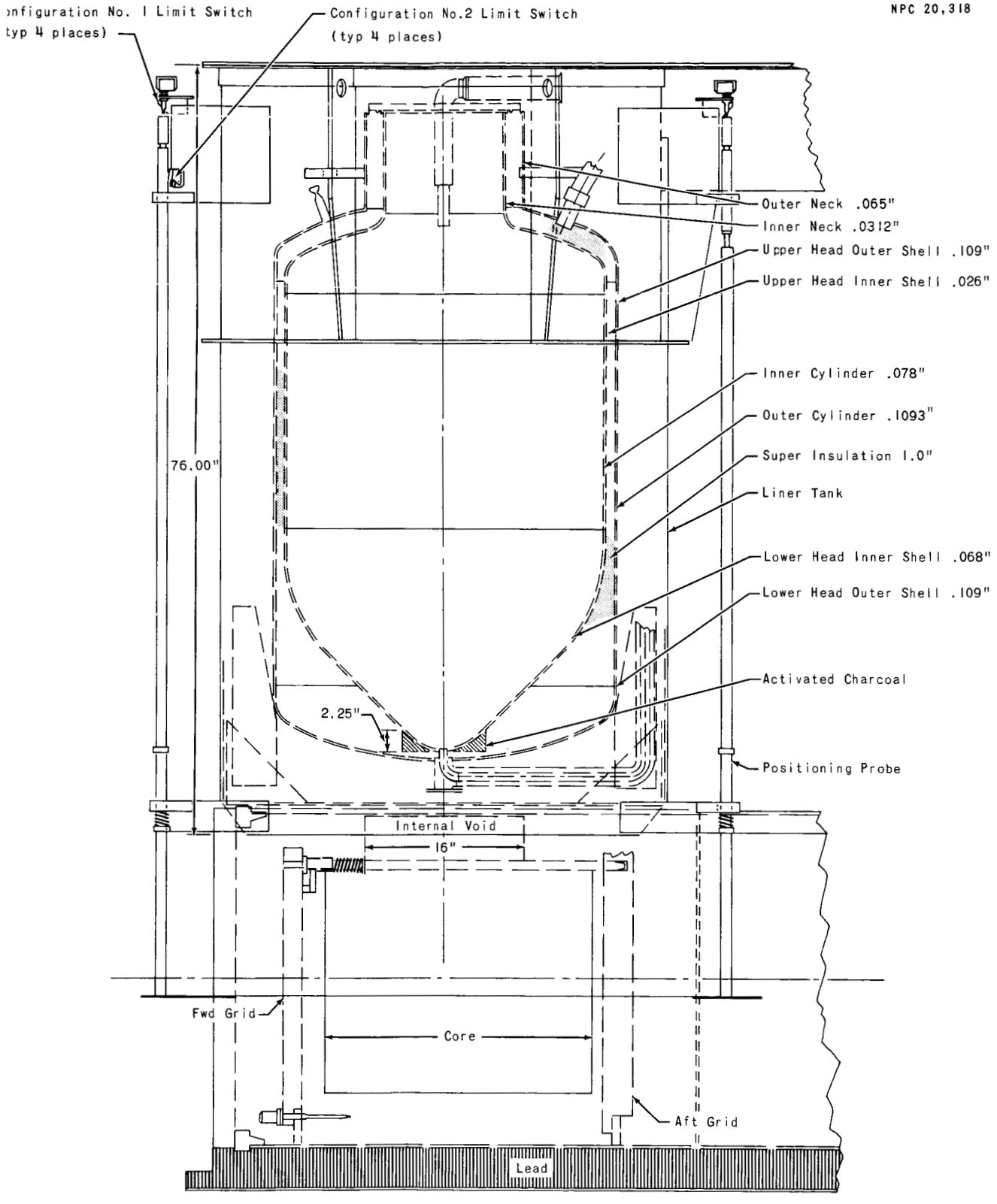

Figure 2 Liquid-Hydrogen-Heating Experimental Geometry

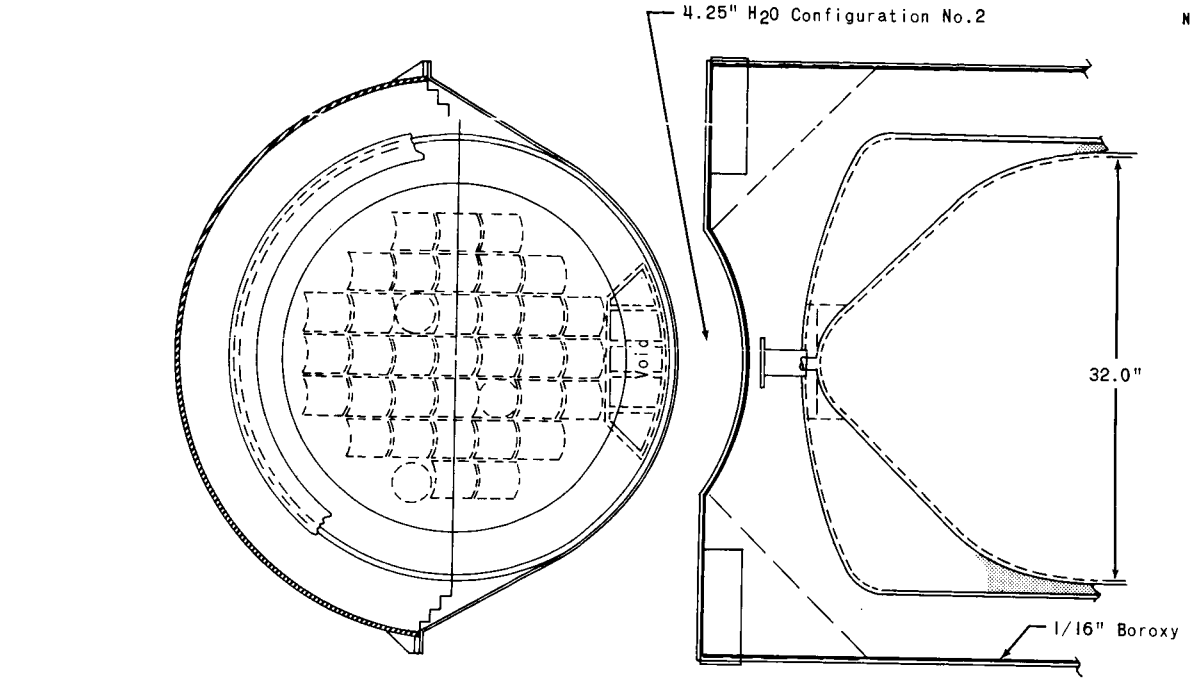

CONFIGURATION No.2

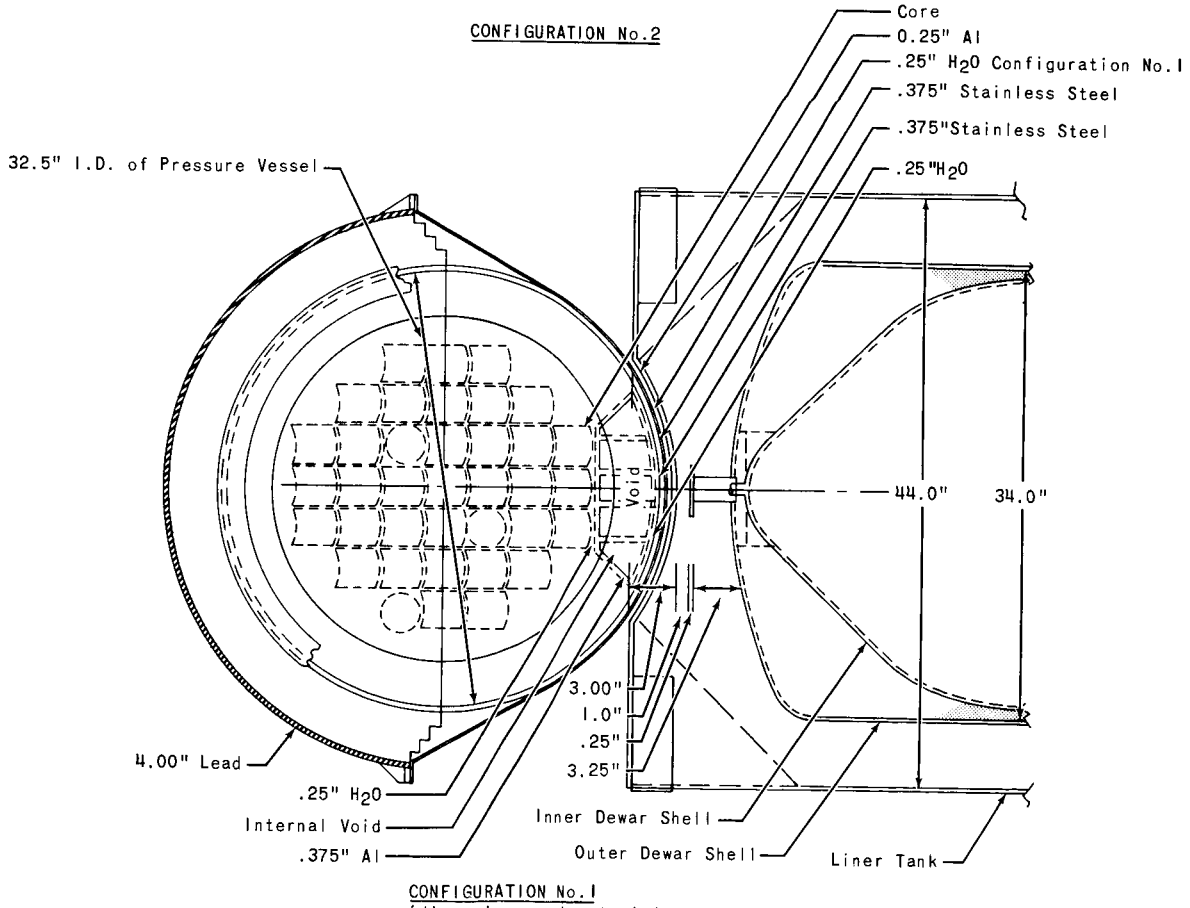

CONFIGURATION No.1
(dimensions and materials same for both configurations)

Figure 3 Liquid-Hydrogen-Heating Experimental Configurations

below the liner tank with $\sim$ 1/4 in. of water between them. In Configuration 2, the reactor was lowered 4 in.; consequently, 4 in. of additional water separated the liner tank bottom and the reactor pressure vessel. The 4 in. of water reduced the neutron-to-gamma ratio of the radiation incident on the LH_2 tank bottom. Thus the two reactor positions provided two nuclear environments for the experiment and analysis. Most data runs were duplicated for each of the two environments.

2.2 Radiation Detectors

The radiation detectors used in the liquid hydrogen were all of the integrating type and were chosen for their compatibility with the cryogenic environment. Cobalt glass was used for gamma-ray dosimeters. The glass was supplied by Bausch and Lomb in rectangular pieces about 19/32- by 1/4-in. and 1/16-in. thick. Each piece of glass was placed in a box of 1/16-in.-thick walls composed of boron-10 and an epoxy binder. These boxes served as low-energy neutron filters and, thus, virtually eliminated any neutron effects in the readings of the dosimeters. The gamma dose was measured by the amount of discoloration of the cobalt glass caused by gamma rays. The amount of discoloration was determined by measuring the transmission of light waves of 390- and 470-mμ wave lengths with a spectrophotometer before and after exposure of the glass to radiation.

Calibration of the dosimeter was performed with a 1.5-kilocurie cobalt-60 gamma source. Calibration curves were obtained at 93°F and -320°F. The two curves differed only slightly, with a maximum difference in the order of 10%. Although the correction

for temperature was rather small, the calibration curve obtained at -320°F (boiling point of liquid nitrogen) was used for the dosimeters exposed in liquid hydrogen.

The reproducibility of the gamma measurements was in the order of ±5%, and the accuracy of the measurements is about ±10%.

The neutron-flux distributions were measured with radioactivants. Radioactivants have long been used for making neutron-flux measurements and are considered to have an accuracy in the order of ±20%. The thermal-neutron flux was measured by the cadmium-difference technique. The thermal or sub-cadmium flux includes neutrons of energy below 0.48 ev, the approximate cadmium cutoff energy for 20-mil cadmium. Gold foils were used as the thermal-neutron detectors. Copper wires were also used to map thermal-neutron profiles in the liquid hydrgen. The magnitudes of the profiles were normalized to the gold-foil measurements.

No temperature corrections were made to the cross sections used in reducing the gold-foil data. What error this might introduce in the magnitude of the thermal-neutron flux measurements cannot be estimated at this time.

The fast-neutron flux measurements were made with sulfur, aluminum, and magnesium by utilizing threshold-type nuclear reactions of each element. These reactions and the approximate effective threshold of each are given below:

$S^{32}(n,p)P^{32}$	2.9 Mev
$Mg^{24}(n,p)Na^{24}$	7.5 Mev
$Al^{27}(n,\alpha)Na^{24}$	8.1 Mev

Although tests indicated that the cryogenic environment produced no adverse physical effect on the pressed sulfur pellets, the pellets were wrapped in aluminum foil as a precautionary measure in the event of shattering or crumbling of the pellet.

After irradiation, all the radioactivants were processed and counted in NARF's semi-automated counting room. The counting data, radiation exposure data, and detector location data were processed by a computer program which resulted in a tabulation of the neutron flux for each detector position. Further details of the computer program, detectors, and calibration procedures and techniques used in conjunction with radioactivants as neutron detectors are given in Reference 1.

2.3 Experimental Procedure

The nuclear-radiation mapping was performed during four different reactor runs. The radiation distribution was measured with the LH_2 tank empty and full of liquid hydrogen (to a height of about 45 in.) for each of the two reactor configurations. The reactor was at power for 30 minutes for each of the runs. The reactor power for each run was dictated by the exposure required by the cobalt-glass dosimeters. Since the gamma-dosimeter exposure requirements fell within the exposure range of the radioactivants, both neutron and gamma measurements were attained for each reactor run.

Figure 4 shows the locations of the neutron and gamma detectors in and around the tank for each of the reactor runs. In the figure, only the x, y-plane positions are shown; the x, z-plane position distances are identical. Gamma and all types of neutron detectors were used at the tank bottom and also at 1.4, 8.4, and 20.4 in.

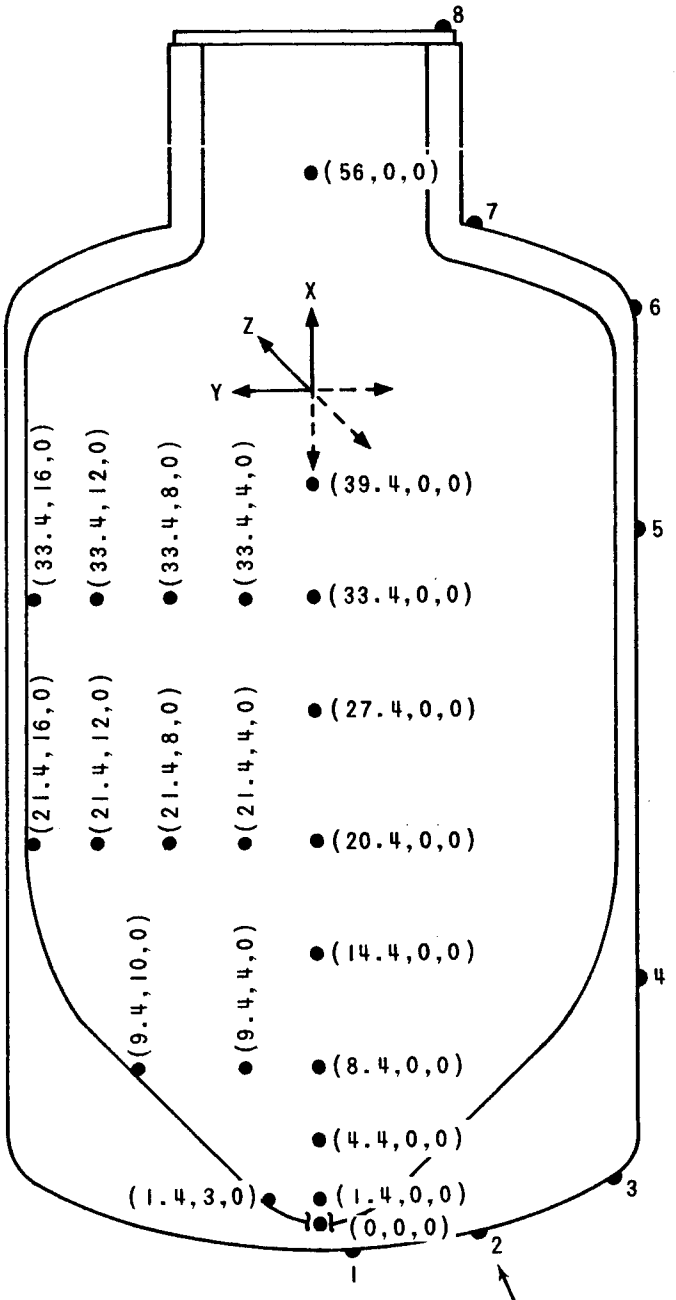

Figure 4 Diagram of Radiation-Detector Positions

from the bottom along the tank centerline. All radiation detectors were used at each position on the outside wall of the LH_2 tank. Only sulfur neutron detectors and cobalt-glass gamma dosimeters were positioned at all other locations. Copper wire to provide thermal-neutron maps was placed along the tank centerline and along each of the foil-holding radial arms supported from the centerline stand. The sulfur pellets and cobalt glass provided adequate maps of the fast-neutron and gamma-ray distributions, respectively, in the tank.

The radiation detectors were packeted between aluminum screen wire and attached to the foil support stand with steel wire. The foil support stand was fabricated of small-diameter stainless-steel rods. A radiation detector assembly in the aluminum screen wire is shown in Figure 5.

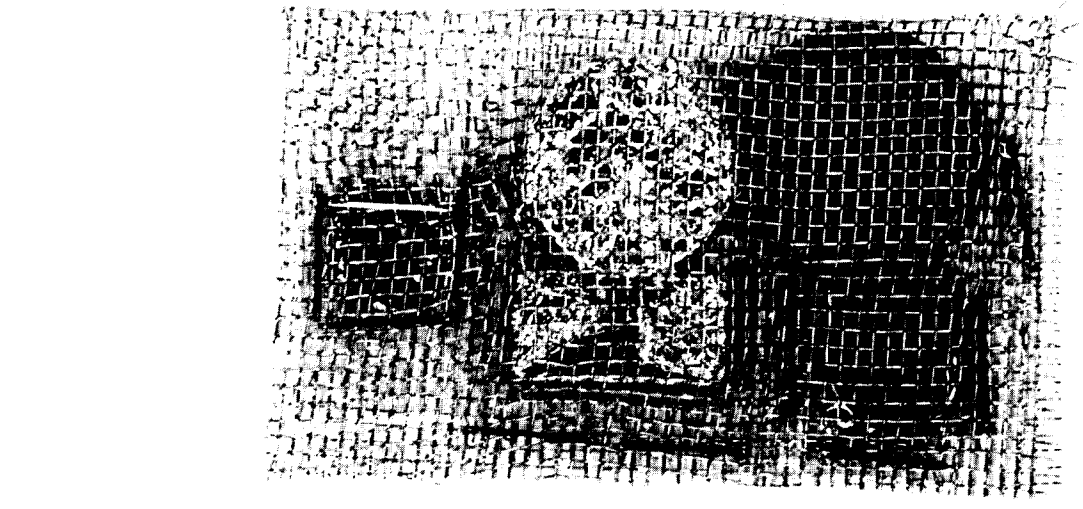

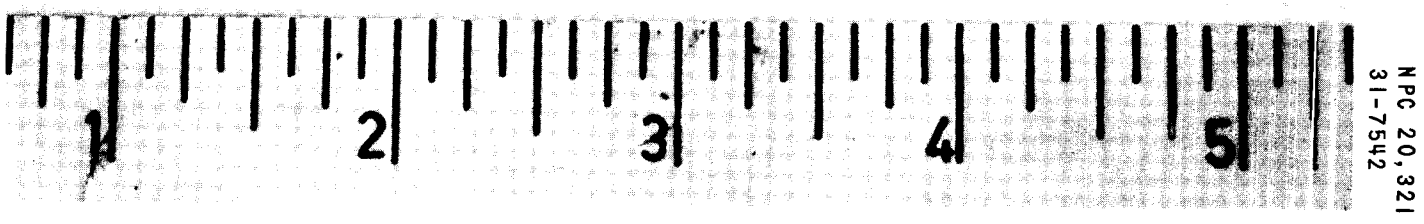

NPC 20,321
31-7542

Figure 5 Detector Packet

3. METHODS OF CALCULATIONS

The analytical calculations were, in the main, performed through extensive use of IBM-7090 digital-computer code C-17 (Ref. 2) developed at NARF. This is a shield penetration program for calculating a modified gamma spectrum and is based on the differential energy spectra obtained by a moments-method solution of the Boltzmann transport equation (Ref. 3). The fast-neutron portion of the program yields a spectrum based upon differential energy spectra calculated by Nuclear Development Corporation of America (NDA) for a point-isotropic fission source in an infinite medium. The fast-neutron results for this analysis were from an NDA calculation representing a moments-method solution of the Boltzmann transport equation for water (Ref. 4).

For these calculations, the source of the nuclear environment, the ASTR, was represented by a total of 126 source points, each of which corresponds to a certain volume element of the core and the power distribution applied thereto. The total power of the reactor core was normalized to one watt for use in the computer program.

Certain geometric limitations on the description of various regions were encountered in the calculational model employed in the shield-penetration program. Specifically, any region which is represented as a solid of revolution must have as its axis of revolution the x-axis in a Cartesian coordinate system. With this in mind it is readily seen from Figures 2 and 3 that, in reality, some cylindrical regions exist which are not adaptable

to this type of geometric definition. For the calculational model, the regions of different materials were defined as precisely as possible. However, in some instances, it was necessary to approximate some curved surfaces by a number of planes. The conical, or bottom, portion of the tank was represented by a series of frusta of cones. For simplification in defining a calculational model, the axis or centerline of the tank was chosen as the x-axis with detector locations, etc. being referenced thereto. For convenience, the coordinate system (see Fig. 4) had as its origin the bottom of the inside of the tank (or a zero liquid level).

Detector locations for which the calculations were made were situated in the x, y plane. Although true symmetry did not exist in the test geometry for the x, y and x, z planes, several calculations were made to determine the variation of dose-rate in the two planes. The difference was extremely small, and the assumption was made that the system was symmetrical in the two planes. Thus, the x, y plane was chosen arbitrarily as the plane in which to make calculations. The detector locations were selected so as to yield a well-defined nuclear map within the liquid hydrogen. In some instances, it was necessary to cross-plot and/or interpolate the calculated data in order to obtain a direct comparison with measured data.

The calculated gamma total dose rates consist of several components considered to be the most probable contributors to the total. It is believed that the major sources of secondary gamma rays have been investigated and also that some of the sources considered yielded results of negligible importance.

The primary gamma dose rate is that resulting from the gamma-leakage flux from the reactor. This leakage flux is due to the prompt-fission and decay gammas in the fuel and to the radiative capture and inelastic scattering of neutrons which occur in all materials in the reactor-core structure.

Secondary gamma rays are considered to be those produced by means of radiative capture of thermal neutrons and inelastic scattering of fast neutrons in materials outside of the reactor core. The capture-gamma source materials investigated for this analysis were the liquid hydrogen and the stainless-steel reactor pressure vessel for both configurations. In addition, the captures produced in the 4 in. of water in Configuration 2 were included. The only source considered for the production of gamma rays by means of inelastic scattering of fast neutrons was the iron in the stainless-steel pressure vessel around the ASTR.

The thermal- and fast-neutron fluxes employed in the calculation of secondary gamma rays produced in the stainless-steel pressure vessel, and the surrounding water for Configuration 2, were obtained from a neutron map of the ASTR pressure vessel made prior to this experiment. This particular mapping was made with the ASTR completely submerged, so that the water appears as an infinite medium. Thus, the calculated fluxes represent perhaps more realistically the Configuration 2 geometry (4 in. of additional water outside the pressure vessel) than the Configuration 1 geometry. From these fluxes measured on the surface of the ASTR pressure vessel, fluxes were obtained by exponental attenuation at the points of interest (source point locations) in the steel and water.

To compute the intensities of the secondary-gamma sources in a particular medium due to neutron capture (n,γ) or neutron inelastic scattering (n,n') reactions, an elemental volume was chosen which was represented by a specific source-point location. The intensity of each source point was then computed from

$$\text{Source Strength} = V\Sigma\Phi$$

where

V = volume associated with a particular source point,

Σ = capture or inelastic cross sections, and

Φ = thermal- or fast-neutron flux (n/cm^2-sec) at the point of interest.

Once the source strengths were computed, they became source terms for the computer program (C-17), and, with the appropriate gamma input spectrum for the secondary event under consideration, their contribution to the gamma dose rate in the liquid hydrogen was calculated.

4. RESULTS

The agreement between the results of measurements and calculations was, in general, well within the accuracies of the measurement and calculational techniques used. Several comparisons of calculations with measurements made inside the tank are given in graphical form. A compilation of both measured and calculated gamma dose rates and neutron fluxes are given in Tables I through VIII. Included in these tables are the measurements made on the outside tank surface.

4.1 Fast-Neutron Flux

4.1.1 Centerline Distributions

Measured and calculated fast-neutron fluxes on the tank centerline for Configuration 1 are shown in Figure 6. Comparisons of fluxes above 2.9 and 8.1 Mev are shown to indicate how well the neutron spectrum was predicted. Agreement of the fluxes above 2.9 Mev is quite good and the agreement of the flux above 8.1 Mev is fair. Thus, the calculated neutron spectrum of Configuration 1 is in fair agreement with the measurements.

Figure 7 shows the measured and calculated fast-neutron fluxes for Configuration 2. Again, the agreement of measured and calculated neutron fluxes above 2.9 Mev is good; however, above 8.1 Mev the calculated flux is about 50% higher than the measured flux. In both Configuations, the calculated neutron spectrum is "harder" that the measurements indicate. No explanation is readily available for this difference.

4.1.2 Radial Distribution

Figure 8 compares the calculated and measured fast-neutron fluxes along the radials from the tank centerline. The C-17 code predicts the magnitude rather well where the scattered-neutron component is small, but the large differences on the upper radials of both Configurations 1 and 2 near the outer periphery of the tank are probably caused by neutrons scattering into the hydrogen from outside the hydrogen tank. These comparisons of calculated data with threshold-detector data were made by integrating the C-17 calculated neutron spectra above 2.9 Mev.

4.2 Thermal-Neutron Flux

The lower neutron-energy cutoff for the C-17 code is 0.33 Mev. Thus, no calculated values are available for comparison with the measured thermal-neutron flux. The measured fluxes obtained with copper wire along the centerline and on the radials are given in Figures 9 and 10, respectively. The magnitudes of these values were normalized to gold-foil values. In Figure 10, the decrease of thermal flux towards the tank wall is assumed to be due to absorbtion of thermal neutrons in the hydrogen tank and liner tank walls.

4.3 Gamma-Ray Dose Rate

4.3.1 Centerline Distributions

A comparison of measured and calculated gamma-ray dose rates on the tank centerline for Configurations 1 and 2 are shown in Figures 11 and 12, respectively. Configuration 1 data agree fairly well, the maximum difference between calculated and measured data being about 20%. The agreement for Configuration 2 is rather poor over the first few inches of liquid hydrogen, where

the calculated data is higher by a maximum difference of approximately 48%. Note that, for the total gamma-ray data for both configurations, the calculated-value curves exhibit a slightly steeper slope than do the measured-value curves. One possible explanation for the difference in slopes is a shortcoming of the use of the differential-energy-spectra data in the penetration program. The basic gamma-buildup data is more realistic (and the results are more reliable) when applied to calculating a modified spectrum after penetration of regions or materials which are of such dimensions as to appear to be infinite. The mass of hydrogen in the tank bottom, or conical portion of the tank, does not appear to be an infinite region of hydrogen. Thus, the calculated dose rates would most probably represent an overestimate of the true gamma dose rate in this vicinity.

4.3.2 Radial Distributions

The plots of the radial gamma dose-rate distributions at two levels are shown in Figure 13 and 14. The fairly large discrepancy between calculated and measured dose rates near the tank wall in Configuration 1 indicates a possible capture component in the walls of the tank or the surrounding water medium. Since the agreement is somewhat closer near the centerline, such a capture component must be in the low energy range in order to be attenuated so rapidly by the hydrogen. This effect is not discernible for Configuration 2 because the neutron-to-gamma ratio is lower and the primary gamma component apparently overshadows the secondary component—which is, after all, lower for Configuration 2.

5. CONCLUSIONS

The use of proven radiation detectors and methods, with a few precautionary techniques for the cryogenic environment, provided satisfactory results. The integrating-type detectors, radioactivants and cobalt glass, were readily adaptable to the cryogenic environment and were small enough to be used in the experiment. The integrating devices, however, limited the nuclear measurements to steady-state conditions, that is, with the liquid level fixed. When physically small rate detectors become available, it will be of considerable interest to continuously monitor radiation intensities as the liquid hydrogen flows from the tank and the liquid level in the tank changes.

The calculated values from the C-17 shield penetration program are in good agreement with the measured values and, consequently, give a measure of confidence to calculations performed in the various nuclear-rocket-system design studies. The comparison of measured and calculated values indicates that even rather simple codes like C-17 can provide results with an accuracy of the order of 20%.

Table I. Calculated Gamma Dose Rates: Configuration I
(r/hr-w)

Detector Coordinates (in.)			Gamma Dose-Rate Components				Total Gamma Dose Rate
x	y	z	Primary Gammas	(n,γ) in LH_2	(n,γ) in Stainless-Steel Pressure Vessel	(n,n') in Iron of Pressure Vessel	
.10	0	0	2.05(0)	7.99(-2)	1.45(0)	7.06(-2)	3.65(0)
1.08	0	0	1.88(0)	1.04(-1)	1.33(0)	6.66(-2)	3.38(0)
3.05	0	0	1.60(0)	1.33(-1)	1.04(0)	5.28(-2)	2.83(0)
5.16	0	0	1.56(0)	1.35(-1)	7.82(-1)	3.98(-2)	2.52(0)
9.84	0	0	1.15(0)	1.01(-1)	4.58(-1)	2.31(-2)	1.73(0)
14.47	0	0	8.49(-1)	6.64(-2)	2.90(-1)	1.44(-2)	1.22(0)
22.00	0	0	5.48(-1)	3.35(-2)	1.60(-1)	7.68(-3)	7.49(-1)
33.79	0	0	3.05(-1)	1.02(-2)	7.78(-2)	3.53(-3)	3.96(-1)
45.00	0	0	1.89(-1)	4.13(-3)	4.55(-2)	1.93(-3)	2.40(-1)
1.08	2.56	0	2.14(0)	8.44(-2)	1.33(0)	6.76(-2)	3.62(0)
3.05	2.56	0	1.81(0)	1.24(-1)	1.00(0)	5.11(-2)	2.99(0)
3.05	4.72	0	1.85(0)	7.45(-2)	9.17(-1)	4.66(-2)	2.89(0)
5.16	2.56	0	1.56(0)	1.32(-1)	7.62(-1)	3.87(-2)	2.49(0)
5.16	4.72	0	1.56(0)	9.27(-2)	7.11(-1)	3.61(-2)	2.40(0)
5.16	6.89	0	1.49(0)	6.38(-2)	6.08(-1)	3.07(-2)	2.19(0)
9.84	4.72	0	1.12(0)	8.38(-2)	4.26(-1)	2.15(-2)	1.65(0)
9.84	6.89	0	1.07(0)	7.15(-2)	3.96(-1)	1.99(-2)	1.56(0)
9.84	9.05	0	1.02(0)	5.49(-2)	3.56(-1)	1.79(-2)	1.45(0)
9.84	11.42	0	9.51(-1)	3.87(-2)	2.97(-1)	1.48(-2)	1.30(0)
14.47	4.72	0	8.21(-1)	5.89(-2)	2.77(-1)	1.38(-2)	1.17(0)
22.00	5.31	0	5.24(-1)	2.96(-2)	1.53(-1)	7.35(-3)	7.14(-1)
22.00	10.63	0	4.88(-1)	2.24(-2)	1.39(-1)	6.64(-3)	6.56(-1)
22.00	15.90	0	4.34(-1)	1.42(-2)	1.17(-1)	5.59(-3)	5.71(-1)
33.79	5.31	0	2.93(-1)	9.58(-3)	7.63(-2)	3.45(-3)	3.82(-1)
33.79	10.63	0	2.77(-1)	8.09(-3)	7.20(-2)	3.24(-3)	3.60(-1)
33.79	15.90	0	2.58(-1)	6.25(-3)	6.56(-2)	2.67(-3)	3.32(-1)

Table II. Calculated Gamma Dose Rates: Configuration II
(r/hr/w)

Detector Coordinates (in.)			Gamma Dose-Rate Components					Gamma Gamma Dose Rate
x	y	z	Primary Gammas	(n,γ) in LH_2	(n,γ) in Stainless-Steel Pressure Vessel	(n,n') in Iron of Pressure Vessel	(n,γ) in 4" H_2O Shield	
.10	0	0	1.08(-0)	1.02(-2)	6.40(-1)	2.63(-2)	4.37(-1)	2.19(0)
5.16	0	0	7.76(-1)	1.75(-2)	3.94(-1)	1.70(-2)	.244(-1)	1.45(0)
14.47	0	0	4.97(-1)	9.69(-3)	1.71(-1)	7.26(-3)	9.56(-2)	7.80(-1)
22.00	0	0	3.31(-1)	5.55(-3)	1.02(-1)	4.21(-3)	5.33(-2)	4.96(-1)
33.79	0	0	1.91(-1)	1.91(-3)	5.32(-2)	2.05(-3)	2.59(-2)	2.74(-1)
45.00	0	0	1.21(-1)	7.45(-4)	3.23(-2)	1.16(-3)	1.48(-2)	1.70(-1)
22.00	5.31	0	3.19(-1)	4.86(-3)	9.92(-2)	4.07(-3)	5.16(-2)	4.79(-1)
22.00	10.63	0	3.02(-1)	3.62(-3)	9.05(-2)	3.69(-3)	4.70(-2)	4.47(-1)
22.00	15.90	0	2.74(-1)	2.25(-3)	7.85(-2)	3.18(-3)	4.08(-2)	3.99(-1)
33.79	5.93	0	1.84(-1)	1.76(-3)	5.23(-2)	2.01(-3)	2.53(-2)	2.65(-1)
33.79	10.63	0	1.77(-1)	1.44(-3)	4.94(-2)	1.89(-3)	2.41(-2)	2.54(-1
33.79	15.90	0	1.67(-1)	1.06(-3)	4.57(-2)	1.74(-3)	2.21(-2)	2.38(-1)

Table III. Calculated Fast-Neutron Spectra: Configuration I

Detector Coordinates (in.)			Fast-Neutron-Flux Spectra (n/cm^2-sec-Mev-w)										Fast-Neutron Flux > 2.9 Mev $\left(\frac{n}{cm^2\text{-sec-w}}\right)$
x	y	z	0.33 Mev	1.0 Mev	2.0 Mev	3.0 Mev	4.0 Mev	6.0 Mev	8.0 Mev	10.0 Mev	14.0 Mev	18.0 Mev	
.10	0	0	4.20(4)	2.50(4)	1.69(4)	1.13(4)	7.19(3)	2.51(3)	6.78(2)	1.54(2)	6.90(0)	1.76(-1)	2.48(4)
5.16	0	0	1.52(4)	8.73(3)	6.19(3)	4.34(3)	2.89(3)	1.08(3)	3.01(2)	6.91(1)	3.60(0)	8.32(-2)	9.68(3)
14.47	0	0	2.48(3)	1.05(3)	8.39(2)	6.57(2)	4.95(2)	2.15(2)	6.78(1)	1.62(1)	1.34(0)	2.79(-2)	1.69(3)
22.00	0	0	7.55(2)	2.39(2)	1.96(2)	1.62(2)	1.33(2)	6.44(1)	2.26(1)	5.63(0)	5.88(-1)	1.19(-2)	4.76(2)
33.79	0	0	9.18(1)	2.93(1)	2.24(1)	2.03(1)	1.83(1)	1.05(1)	4.30(0)	1.16(0)	8.58(-2)	1.63(-3)	7.11(1)
45.00	0	0	8.68(0)	4.48(0)	3.29(0)	3.13(0)	2.93(0)	2.02(0)	9.29(-1)	2.64(-1)	7.90(-3)	1.28(-4)	1.28(1)
22.00	5.31	0	7.47(2)	2.45(2)	2.00(2)	1.65(2)	1.35(2)	6.48(1)	2.26(1)	5.61(0)	5.59(-1)	1.13(-2)	4.95(2)
22.00	10.63	0	8.46(2)	2.93(2)	2.39(2)	1.95(2)	1.56(2)	7.33(1)	2.50(1)	6.15(0)	5.97(-1)	1.21(-2)	5.68(2)
22.00	15.90	0	1.09(3)	4.18(2)	3.36(2)	2.68(2)	2.08(2)	9.37(1)	3.07(1)	7.42(0)	6.87(-1)	1.42(-2)	7.47(2)
33.79	5.31	0	9.32(1)	2.90(1)	2.23(1)	2.01(1)	1.81(1)	1.04(1)	4.22(0)	1.14(0)	8.82(-2)	1.68(-3)	7.22(1)
33.79	10.63	0	1.02(2)	3.07(1)	2.37(1)	2.12(1)	1.90(1)	1.08(1)	4.37(0)	1.17(0)	9.71(-2)	1.87(-3)	7.55(1)
33.79	15.90	0	1.17(2)	3.42(1)	2.67(1)	2.36(1)	2.10(1)	1.16(1)	4.65(0)	1.23(0)	1.12(-1)	2.19(-3)	8.23(1)

Table IV. Calculated Fast-Neutron Spectra: Configuration II

Detector Coordiaates (in.)			Fast-Neutron-Flux Spectra (n/cm^2-sec-Mev-w)										Fast-Neutron Flux > 2.9 Mev $\left(\frac{n}{cm^2\text{-sec-w}}\right)$
x	y	z	0.33 Mev	1.0 Mev	2.0 Mev	3.0 Mev	4.0 Mev	6.0 Mev	8.0 Mev	10.0 Mev	14.0 Mev	18.0 Mev	
.10	0	0	7.34(3)	3.57(3)	2.76(3)	2.09(3)	1.51(3)	6.25(2)	1.88(2)	4.40(1)	3.09(0)	6.56(-2)	5.11(3)
5.16	0	0	3.00(3)	1.19(3)	9.62(2)	7.63(2)	5.86(2)	2.60(2)	8.35(1)	2.00(1)	1.76(0)	3.64(-2)	2.01(3)
14.47	0	0	7.13(2)	2.13(2)	1.74(2)	1.46(2)	1.22(2)	6.08(1)	2.21(1)	5.56(0)	5.9 (-1)	1.20(-2)	4.41(2)
22.00	0	0	1.88(2)	5.49(1)	4.28(1)	3.79(1)	3.37(1)	1.87(1)	7.45(0)	1.98(0)	1.78(-1)	3.45(-3)	1.28(2)
33.79	0	0	1.44(1)	7.31(0)	5.36(0)	5.11(0)	4.77(0)	3.19(0)	1.43(0)	4.06(-1)	1.22(-2)	1.97(-4)	2.06(1)
45.00	0	0	2.32(0)	1.27(0)	9.36(-1)	8.87(-1)	8.41(-1)	6.37(-1)	3.24(-1)	9.50(-2)	2.77(-3)	4.68(-5)	4.52(0)
22.00	5.31	0	2.01(2)	5.81(1)	4.57(1)	4.01(1)	3.54(1)	1.94(1)	7.66(0)	2.02(0)	1.91(-1)	3.76(-3)	1.38(2)
22.00	10.63	0	2.61(2)	7.52(1)	6.00(1)	5.18(1)	4.51(1)	2.39(1)	9.17(0)	2.38(0)	2.41(-1)	4.81(-3)	1.73(2)
22.00	15.90	0	3.97(2)	1.23(2)	9.98(1)	8.40(1)	7.04(1)	3.52(1)	1.28(1)	3.23(0)	3.22(-1)	6.46(-3)	2.63(2))
33.79	5.31	0	1.46(1)	7.37(0)	5.40(0)	5.15(0)	4.80(0)	3.19(0)	1.42(0)	4.04(-1)	1.22(-2)	1.96(-4)	2.08(1)
33.79	10.63	0	1.77(1)	8.31(0)	6.12(0)	5.79(0)	5.38(0)	3.51(0)	1.55(0)	4.37(-1)	1.48(-2)	2.41(-4)	2.30(1)
33.79	15.90	0	2.38(1)	1.01(1)	7.45(0)	7.00(0)	6.46(0)	4.09(0)	1.77(0)	4.95(-1)	2.02(-2)	3.42(-4)	2.72(1)

TABLE V. RADIATION MEASUREMENTS INSIDE EMPTY TANK

For Positions where All Detectors Were Used

Detector Coordinates (in.)			Gamma Dose Rate	Neutron Flux Data (n/cm^2-sec-w)				Cd Ratio
				S	Mg	Al	Au	
x	y	z	Co Glass (r/hr-w)	>2.9 Mev	>7.5 Mev	>8.1 Mev	Thermal	
				Configuration 1				
0	0	0	2.82(0)	-	3.54(3)	9.45(2)	5.48(3)	1.12
1.4	0	0	3.34(0)	9.34(3)	3.09(3)	8.01(2)	-	-
8.4	0	0	2.04(0)	1.66(4)	1.80(3)	5.02(2)	2.59(3)	1.10
20.4	0	0	1.14(0)	7.99(3)	1.05(3)	2.47(2)	5.08(3)	1.47
				Configuration 2				
0	0	0	1.50(0)	1.82(3)	6.73(2)	2.19(2)	3.04(1)	1.01
1.4	0	0	1.63(0)	4.79(3)	6.73(2)	2.09(2)	-	-
8.4	0	0	1.11(0)	3.12(3)	4.05(2)	1.32(2)	1.66(2)	1.06
20.4	0	0	6.19(-1)	1.66(3)	2.43(2)	7.10(1)	3.42(2)	1.21

For Positions Where Cobalt Glass and Sulfur Were Used

Detector Coordinates (in.)			Configuration 1		Configuration 2	
			Co Glass	S	Co Glass	S
x	y	z	(r/hr-w)	(n/cm^2-sec-w)	(r/hr-w)	(n/cm^2-sec-w)
4.4	0	0	2.62(0)	2.36(4)	1.37(0)	4.06(3)
14.4	0	0	1.51(0)	1.07(4)	-	2.34(3)
27.4	0	0	8.62(-1)	-	4.88(-1)	1.18(3)
39.4	0	0	5.96(-1)	3.40(3)	3.34(-1)	7.82(2)
56.0	0	0	3.84(-1)	2.24(3)	2.25(-1)	5.18(2)
1.4	3	0	3.42(0)	3.23(4)	-	5.58(3)
9.4	4	0	1.83(0)	1.43(4)	1.01(0)	2.92(3)
9.4	10	0	1.71(0)	1.24(4)	9.76(-1)	2.72(3)
21.4	4	0	1.05(0)	7.37(3)	-	1.50(3)
21.4	8	0	9.96(-1)	6.88(3)	3.64(-1)	1.57(3)
21.4	12	0	1.00(0)	6.80(3)	5.70(-1)	1.48(3)
21.4	16	0	9.25(-1)	-	-	1.40(3)
33.4	4	0	6.74(-1)	4.37(3)	3.90(-1)	9.92(2)
33.4	8	0	5.76(-1)	4.35(3)	3.86(-1)	9.54(2)
33.4	12	0	6.66(-1)	3.98(3)	3.75(-1)	8.94(2)
33.4	16	0	6.66(-1)	3.99(3)	3.90(-1)	9.69(2)
1.4	0	3	3.21(0)	3.18(4)	1.71(0)	5.63(3)
9.4	0	4	1.80(0)	1.48(4)	9.87(-1)	2.88(3)
9.4	0	10	1.71(0)	1.17(4)	9.00(-1)	2.39(3)
21.4	0	4	1.07(0)	7.45(3)	6.15(-1)	1.63(3)
21.4	0	8	1.04(0)	6.66(3)	-	1.50(3)
21.4	0	12	9.02(-1)	6.17(3)	5.48(-1)	1.37(3)
21.4	0	16	9.02(-1)	5.66(3)	5.18(-1)	1.14(3)
33.4	0	4	6.82(-1)	4.28(3)	3.71(-1)	9.59(2)
33.4	0	8	6.98(-1)	4.33(3)	3.75(-1)	9.78(2)
33.4	0	12	6.70(-1)	3.97(3)	-	9.26(2)
33.4	0	16	6.51(-1)	3.77(3)	3.23(-1)	8.41(2)

TABLE VI. RADIATION MEASUREMENTS INSIDE LH_2-FILLED TANK

For Positions Where All Detectors Were Used

Detector Coordinates (in.)			Gamma Dose Rate	Neutron Flux Data (n/cm^2-sec-w)				Cd Ratio
				S	Mg	Al	Au	
x	y	z	Co Glass (r/hr-w)	>2.9 Mev	>7.5 Mev	>8.1 Mev	Thermal	
				Configuration 1				
0	0	0	3.08(0)	2.47(4)	-	8.90(2)	1.56(5)	3.24
1.4	0	0	2.70(0)	1.82(4)	-	6.51(2)	1.94(5)	4.94
8.4	0	0	1.82(0)	4.58(3)	3.89(2)	2.07(2)	1.01(5)	12.6
20.4	0	0	8.24(-1)	-	5.39(1)	3.36(1)	1.29(4)	21.7
				Configuration 2				
0	0	0	1.49(0)	4.45(3)	3.82(2)	2.12(2)	1.75(4)	3.59
1.4	0	0	1.34(0)	3.25(3)	2.93(2)	1.64(2)	2.40(4)	26.3
8.4	0	0	9.43(-1)	9.18(2)	9.91(1)	5.89(1)	1.34(4)	10.6
20.4	0	0	5.09(-1)	1.28(2)	2.00(1)	8.86(0)	2.40(3)	19.8

For Positions Where Cobalt Glass and Sulfur Were Used

Detector Coordinates (in.)			Configuration 1		Configuration 2	
			Co Glass (r/hr-w)	S (n/cm^2-sec-w)	Co Glass (r/hr-w)	S (n/cm^2-sec-w)
x	y	z				
4.4	0	0	2.36(0)	1.06(4)	1.15(0)	1.95(3)
14.4	0	0	1.25(0)	-	6.60(-1)	3.42(2)
27.4	0	0	6.01(-1)	2.35(2)	3.58(-1)	4.55(1)
39.4	0	0	3.64(-1)	4.05(1)	2.26(-1)	1.27(1)
56.0	0	0	2.24(-1)	4.61(1)	1.32(-1)	1.42(1)
1.4	3	0	3.05(0)	2.65(4)	1.51(0)	-
9.4	4	0	1.24(0)	1.54(3)	8.49(-1)	8.42(2)
9.4	10	0	9.12(-1)	5.97(2)	8.49(-1)	1.65(3)
21.4	4	0	8.05(-1)	4.47(2)	4.34(-1)	1.08(2)
21.4	8	0	7.78(-1)	5.19(2)	4.53(-1)	1.19(2)
21.4	12	0	8.24(-1)	6.46(2)	4.34(-1)	1.55(2)
21.4	16	0	8.24(-1)	-	4.15(-1)	2.15(2)
33.4	4	0	4.87(-1)	7.56(1)	2.64(-1)	2.12(1)
33.4	8	0	4.41(-1)	8.50(1)	2.64(-1)	2.31(1)
33.4	12	0	4.67(-1)	1.07(2)	2.64(-1)	3.25(1)
33.4	16	0	4.60(-1)	-	2.45(-1)	4.96(1)
1.4	0	3	2.97(0)	2.41(4)	1.55(0)	4.32(3)
9.4	0	4	1.72(0)	4.19(3)	8.49(-1)	7.86(2)
9.4	0	10	1.53(0)	6.58(3)	8.11(-1)	-
21.4	0	4	8.05(-1)	4.58(2)	4.53(-1)	1.06(2)
21.4	0	8	8.43(-1)	5.05(2)	-	1.12(2)
21.4	0	12	8.05(-1)	5.77(2)	4.34(-1)	1.30(2)
21.4	0	16	8.05(-1)	6.11(2)	4.15(-1)	1.40(2)
33.4	0	4	4.75(-1)	7.42(1)	2.64(-1)	2.18(1)
33.4	0	8	4.60(-1)	7.99(1)	2.64(-1)	2.28(1)
33.4	0	12	4.60(-1)	9.69(1)	2.64(-1)	2.77(1)
33.4	0	16	4.48(-1)	1.40(2)	2.64(-1)	3.89(1)

Table VII. Radiation Measurements on Outside Surface of Empty Tank

Detector Position	Gamma Dose Rate	Neutron Flux Data (n/cm^2-sec-w)				Cd Ratio
		S	Mg	Al	Au	
	Co Glass (r/hr-w)	> 2.9 Mev	> 7.5 Mev	> 8.1 Mev	Thermal	
		Configuration 1				
x,y -Plane - 1	6.12(0)	-	4.84(3)	1.72(3)	9.66(3)	1.20
2	3.14(0)	1.79(4)	2.34(3)	6.00(2)	4.37(3)	1.21
3	1.65(0)	7.55(3)	1.17(3)	2.50(2)	1.07(3)	1.11
4	8.78(-1)	5.22(3)	7.39(2)	1.63(2)	-	-
5	3.53(-1)	2.24(3)	3.52(2)	6.77(1)	1.15(3)	1.25
6	2.35(-1)	1.50(3)	2.26(2)	4.40(1)	4.16(3)	2.17
7	3.18(-1)	2.10(3)	2.64(2)	6.23(1)	2.59(3)	1.69
8	3.14(-1)	2.08(3)	2.27(2)	6.32(1)	2.38(3)	1.56
x, y-Plane - 1	7.76(0)	-	-	1.85(3)	-	-
2	4.36(0)	2.71(4)	2.88(3)	7.80(2)	5.54(3)	1.20
3	-	1.45(4)	1.61(3)	4.14(2)	1.52(3)	1.08
4	1.10(0)	7.54(3)	8.95(2)	2.36(2)	-	-
5	3.22(-1)	2.48(3)	3.52(2)	7.39(1)	9.19(2)	1.21
6	2.43(-1)	1.67(3)	1.98(2)	5.09(1)	3.61(3)	1.95
7	3.41(-1)	2.21(3)	2.49(2)	6.27(1)	2.35(3)	1.54
8	2.71(-1)	2.04(3)	2.77(2)	6.07(1)	2.10(3)	1.60
		Configuration 2				
x, y-Plane - 1	3.04(0)	9.05(3)	1.08(3)	3.48(2)	-	-
2	1.69(0)	3.26(3)	4.62(2)	1.52(2)	3.34(2)	1.16
3	9.38(-1)	1.50(3)	2.56(2)	7.18(1)	2.61(2)	1.24
4.	4.50(-1)	1.01(3)	1.60(2)	4.76(1)	1.32(2)	1.13
5	1.84(-1)	4.54(2)	7.90(1)	2.05(1)	2.16(2)	1.39
6	1.46(-1)	4.00(2)	6.05(1)	1.53(1)	4.67(2)	2.07
7	-	3.98(2)	-	1.72(1)	4.16(2)	2.08
8	-	4.69(2)	6.85(1)	1.90(1)	3.01(2)	1.51
x, y-Plane - 1	3.36(0)	9.92(3)	1.48(3)	4.24(2)	-	-
2	2.29(0)	5.54(3)	7.39(2)	2.32(2)	1.47(3)	1.46
3	-	3.01(3)	1.38(2)	1.31(2)	5.36(2)	1.30
4	-	1.56(3)	2.24(2)	6.94(1)	-	-
5	-	5.13(2)	7.83(1)	2.17(1)	1.53(2)	1.30
6	1.50(-1)	4.53(2)	6.41(1)	1.70(1)	4.92(2)	2.04
7	1.61(-1)	4.10(2)	-	1.80(1)	4.18(2)	2.11
8	3.64(-1)	4.91(2)	6.87(1)	1.96(1)	2.37(2)	1.42

Table VIII. Radiation Measurements on Outside Surface of LH_2-Filled Tank

Detector Position	Gamma Dose Rate	Neutron Flux Data (n/cm^2-sec-w)				Cd Ratio
		S	Mg	Al	Au	
	Co Glass (r/hr-w)	>2.9 Mev	>7.5 Mev	>8.1 Mev	Thermal	
		Configuration 1				
x, y-Plane - 1	6.51(0)	-	-	1.77(3)	-	
2	2.78(0)	1.68(4)	9.02(2)	5.15(2)	2.05(4)	3.63
3	1.55(0)	7.47(3)	5.16(2)	2.45(2)	-	-
4	8.05(-1)	5.16(3)	3.18(2)	1.72(2)	-	
5	2.38(-1)	2.14(2)	2.00(1)	7.01(0)	1.20(3)	8.39
6	1.42(-1)	8.13(1)	8.85(0)	1.69(0)	6.29(1)	2.02
7	1.92(-1)	4.78(1)	6.66(0)	3.15(0)	6.24(2)	16.5
8	1.34(-1)	3.90(1)	6.67(0)	6.14(-1)	5.12(2)	18.1
x, y-Plane - 1	5.94(0)	-	2.72(3)	1.48(3)	1.03(4)	1.12
2	3.49(0)	2.47(4)	1.33(3)	7.27(2)	-	
3	1.65(0)	8.98(3)	5.65(2)	3.09(2)	-	
4	9.00(-1)	5.58(3)	3.79(2)	1.99(2)	2.75(3)	1.42
5	2.34(-1)	2.51(2)	2.09(1)	4.02(0)	-	
6	1.61(-1)	8.45(1)	9.11(0)	4.18(0)	-	
7	2.11(-1)	5.02(1)	6.80(0)	1.16(0)	1.01(2)	11.8
8	1.28(-1)	4.20(1)	-	8.37(-1)	-	
		Configuration 2				
x, y-Plane - 1	2.64(0)	8.45(3)	5.53(2)	3.35(2)	6.06(2)	1.12
2	1.53(0)	2.94(3)	2.32(2)	1.44(2)	8.66(2)	1.51
3	9.06(-1)	1.46(3)	1.22(2)	6.96(1)	5.77(2)	1.48
4	4.53(-1)	9.24(2)	8.41(1)	4.81(1)	4.12(2)	1.50
5	1.40(-1)	6.09(0)	6.41(0)	2.59(0)	7.03(1)	1.72
6	8.49(-2)	2.28(1)	2.13(0)	-	1.16(2)	3.28
7	1.15(-1)	1.28(1)	-	-	5.86(1)	2.62
8	7.36(-2)	7.75(0)	-	1.13(0)	-	-
x, y-Plane - 1	2.45(0)	8.14(3)	5.09(2)	3.09(2)	-	-
2	-	1.08(3)	3.67(2)	2.22(2)	-	-
3	1.00(0)	2.42(3)	2.03(2)	1.23(2)	-	-
4	5.28(-1)	1.32(3)	1.10(2)	6.64(1)	4.03(2)	1.58
5	1.28(-1)	5.81(1)	6.80(0)	-	1.64(2)	1.44
6	1.02(-1)	2.20(1)	2.85(0)	-	6.85(1)	2.32
7	1.15(-1)	1.55(1)	-	1.02(0)	8.81(1)	11.5
8	7.36(-2)	1.23(1)	1.40(0)	7.96(-1)	4.54(1)	2.30

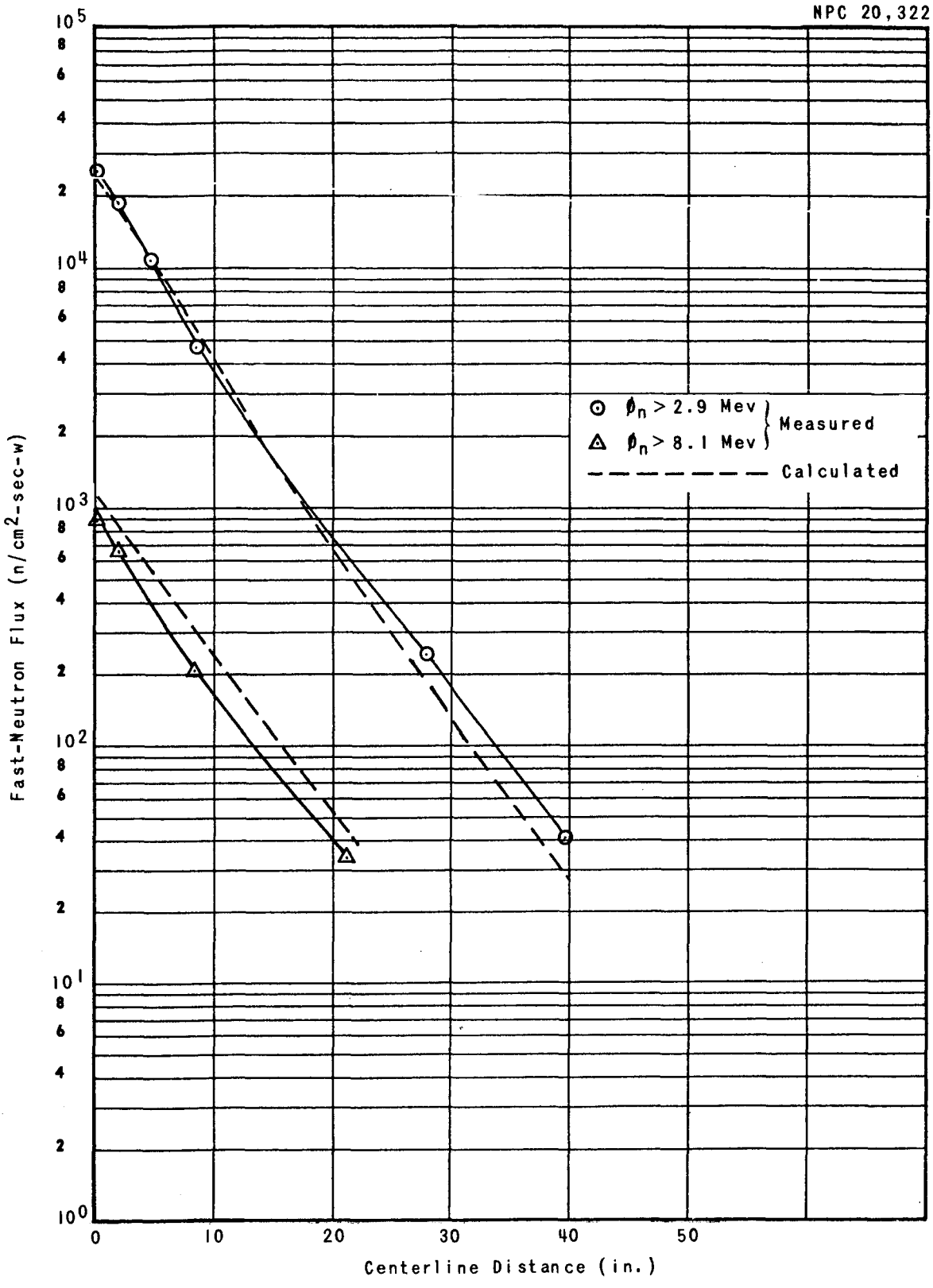

Figure 6 Fast-Neutron Flux Distribution along Centerline: Configuration I

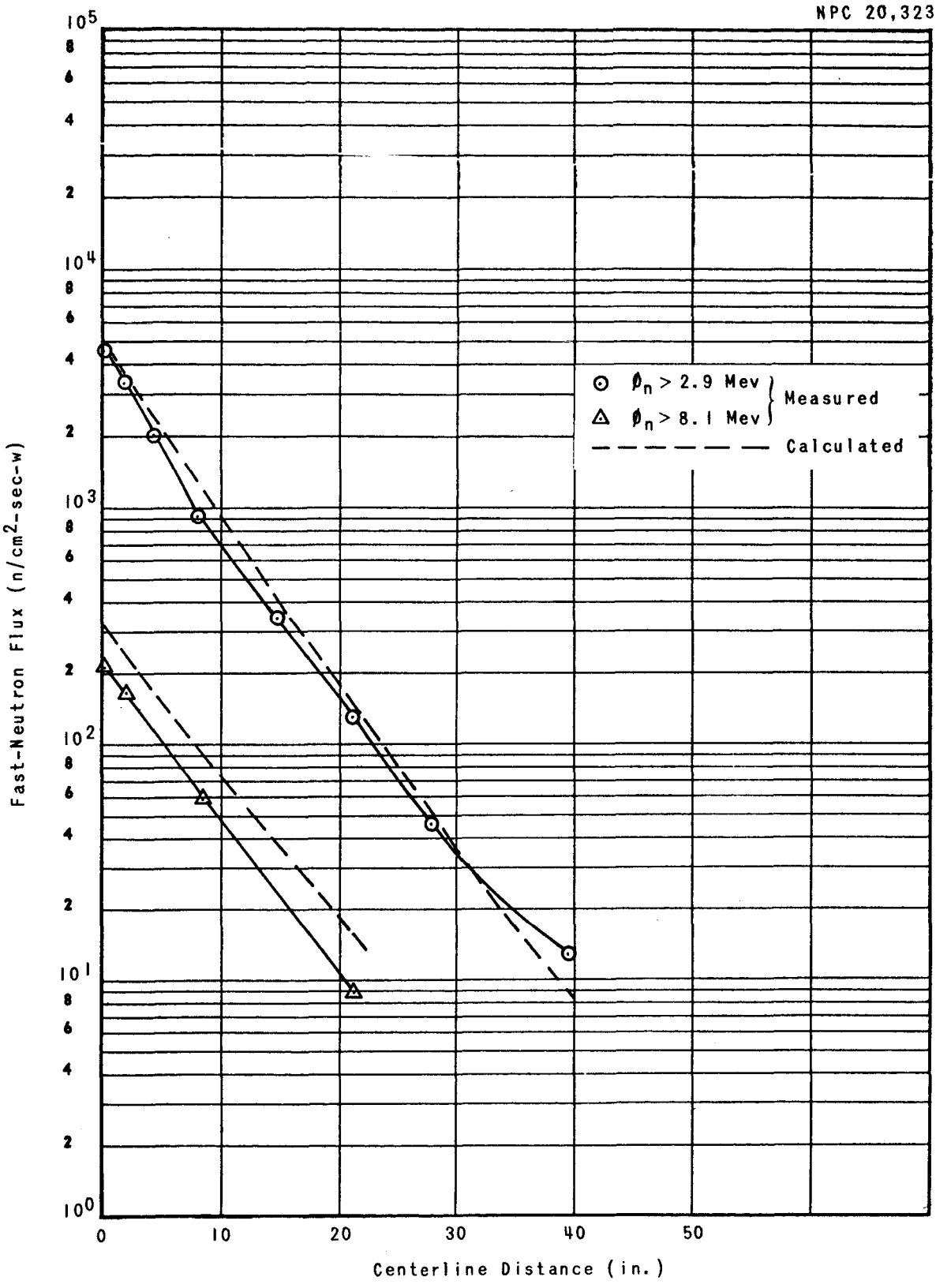

Figure 7 Fast-Neutron Flux Distribution along Centerline: Configuration 2

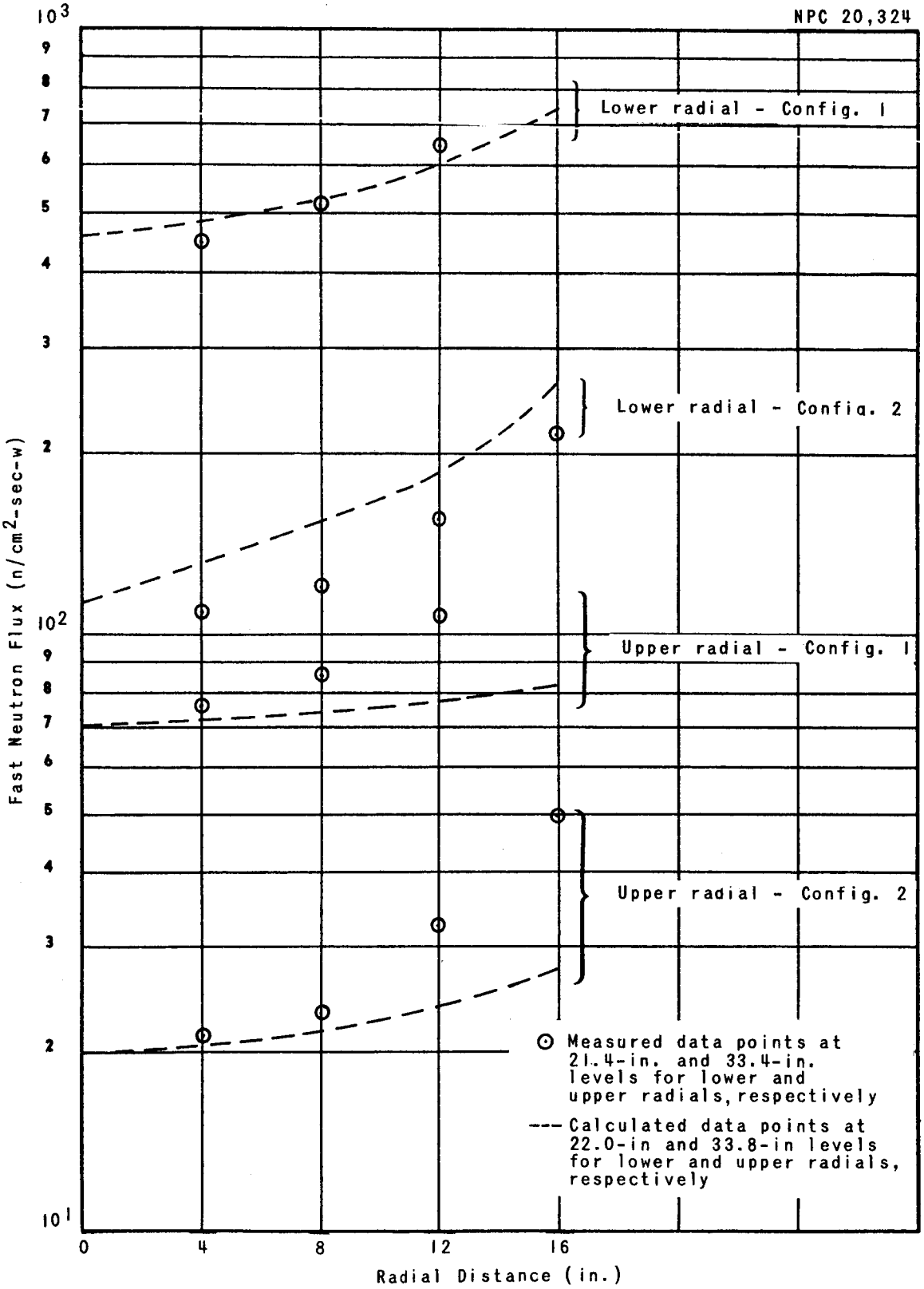

Figure 8. Fast-Neutron Flux Distribution along Upper and Lower Radials

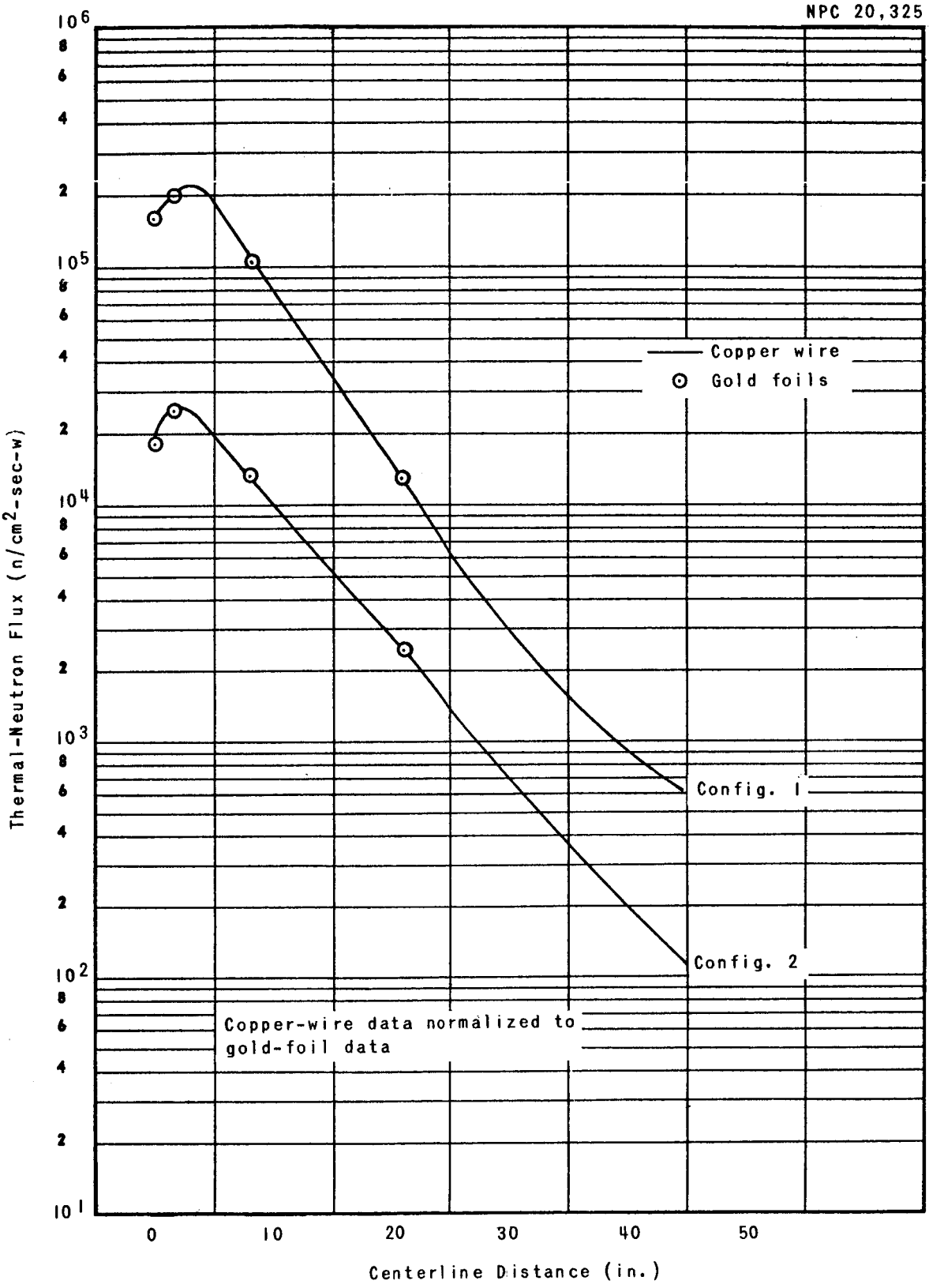

Figure 9 Thermal-Neutron Flux Distribution along Centerline

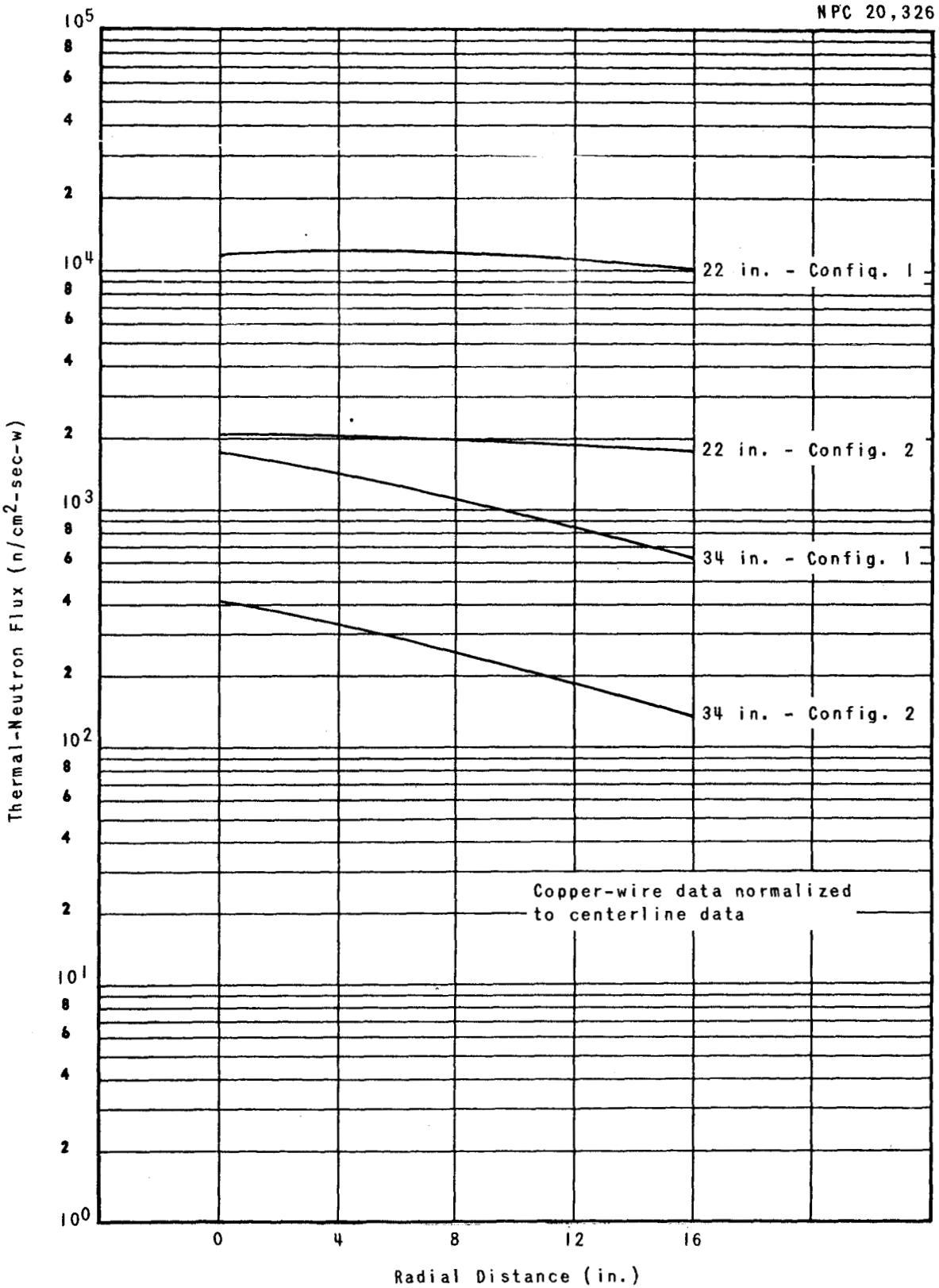

Figure 10 Thermal-Neutron Flux Distribution along Upper and Lower Radials

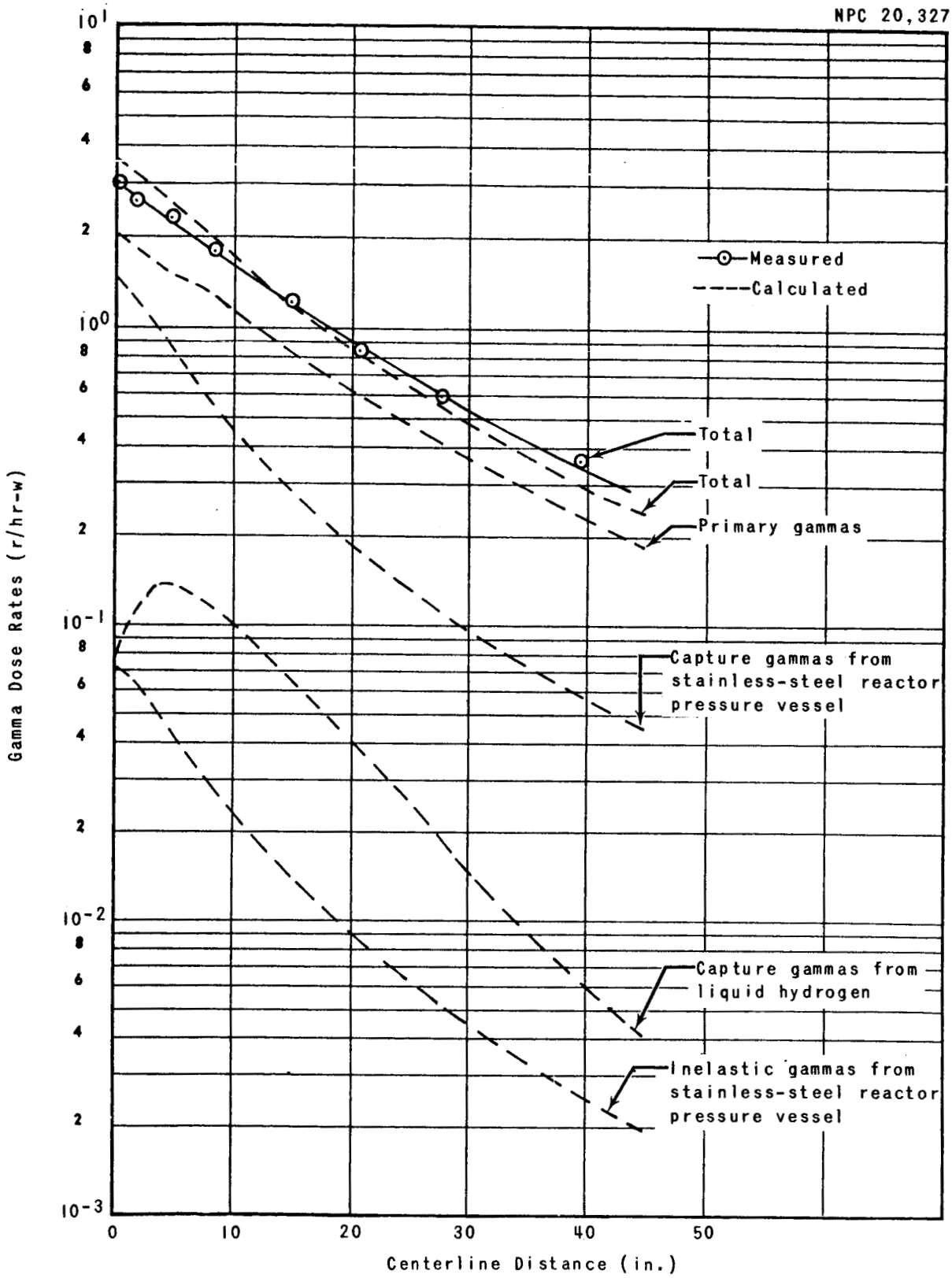

Figure II Gamma Dose-Rate Distribution along Centerline: Configuration I

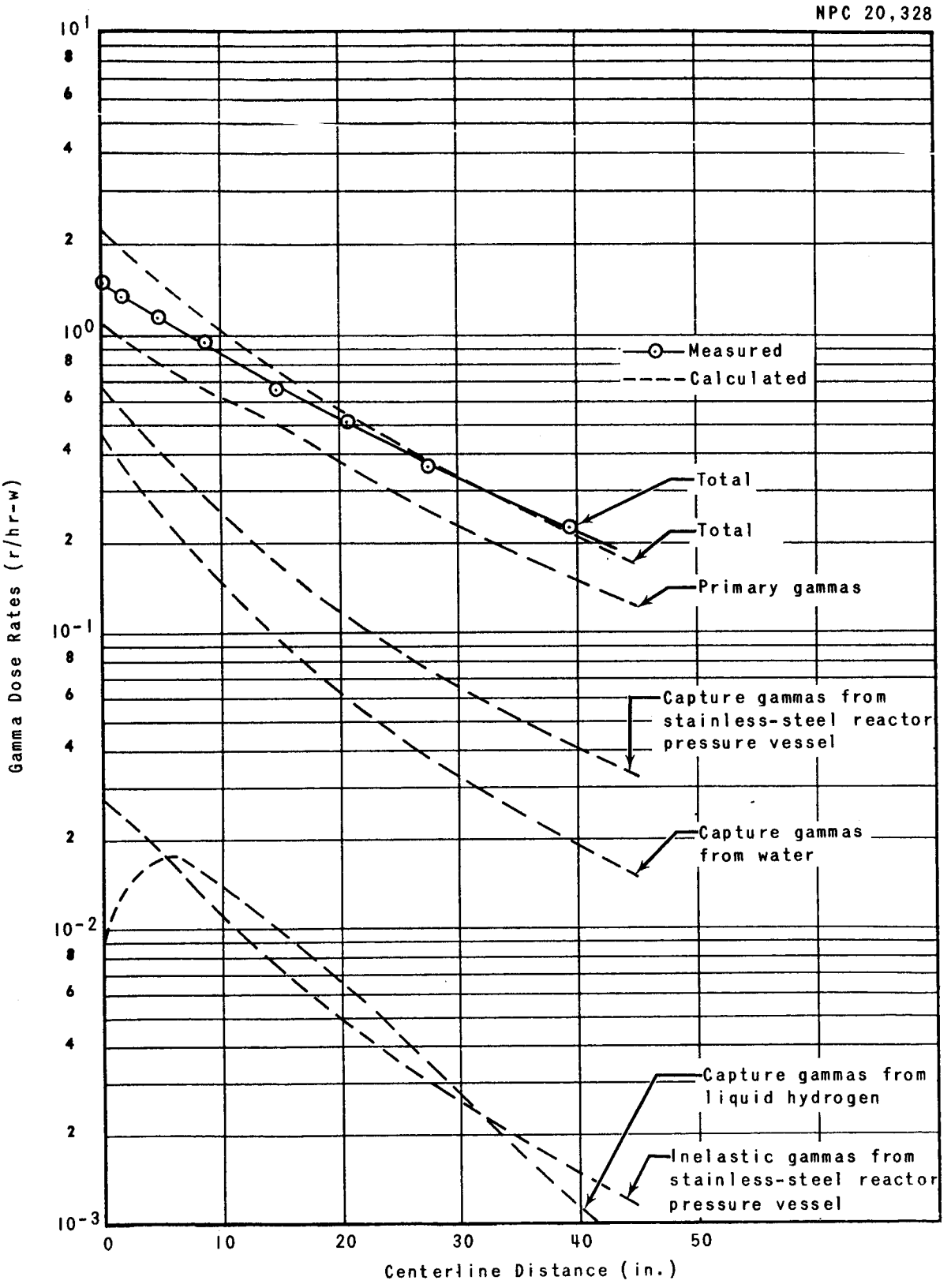

Figure 12 Gamma Dose-Rate Distribution along Centerline: Configuration 2

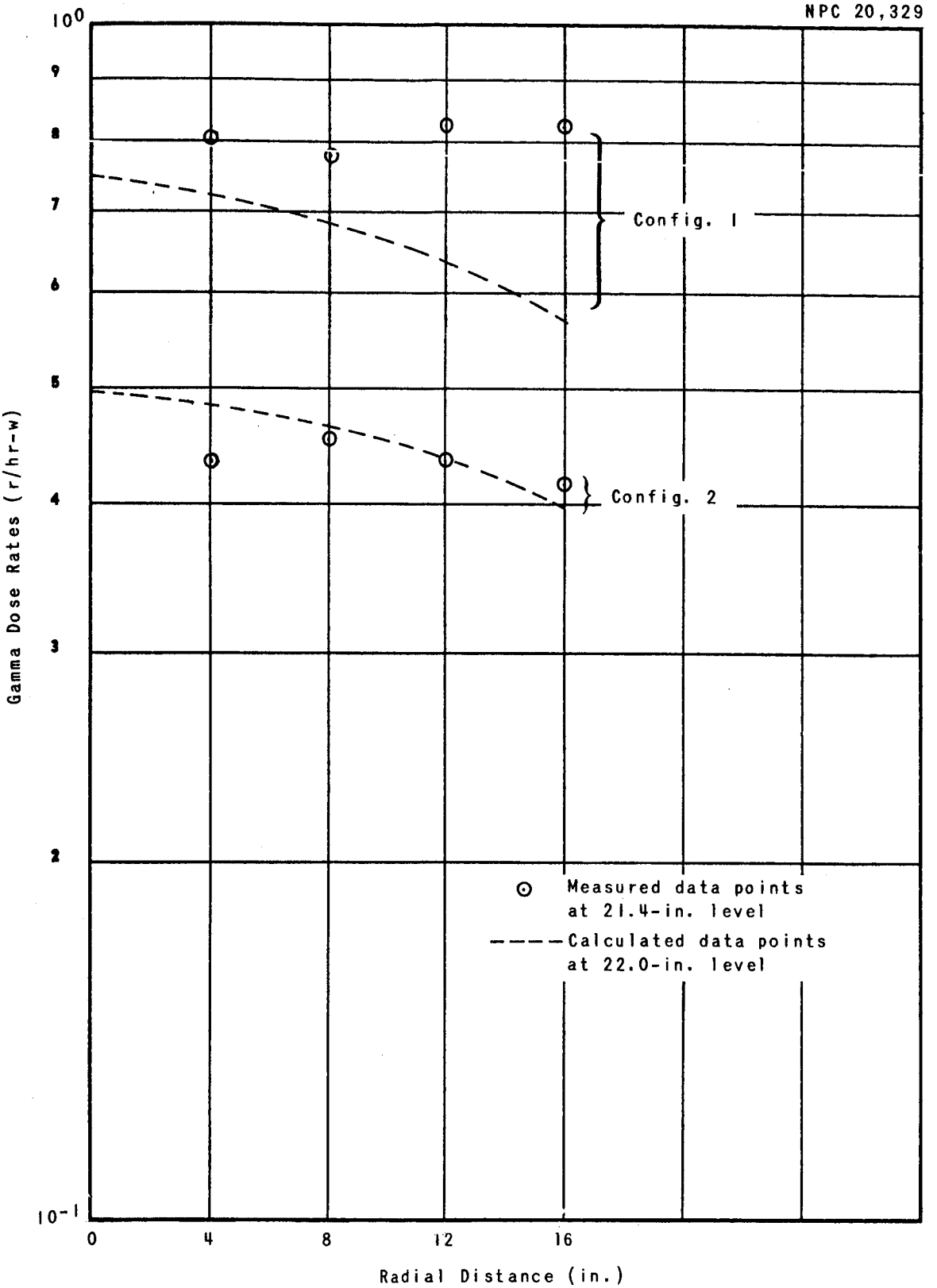

Figure 13 Total Gamma Dose-Rate Distribution along Lower Radial

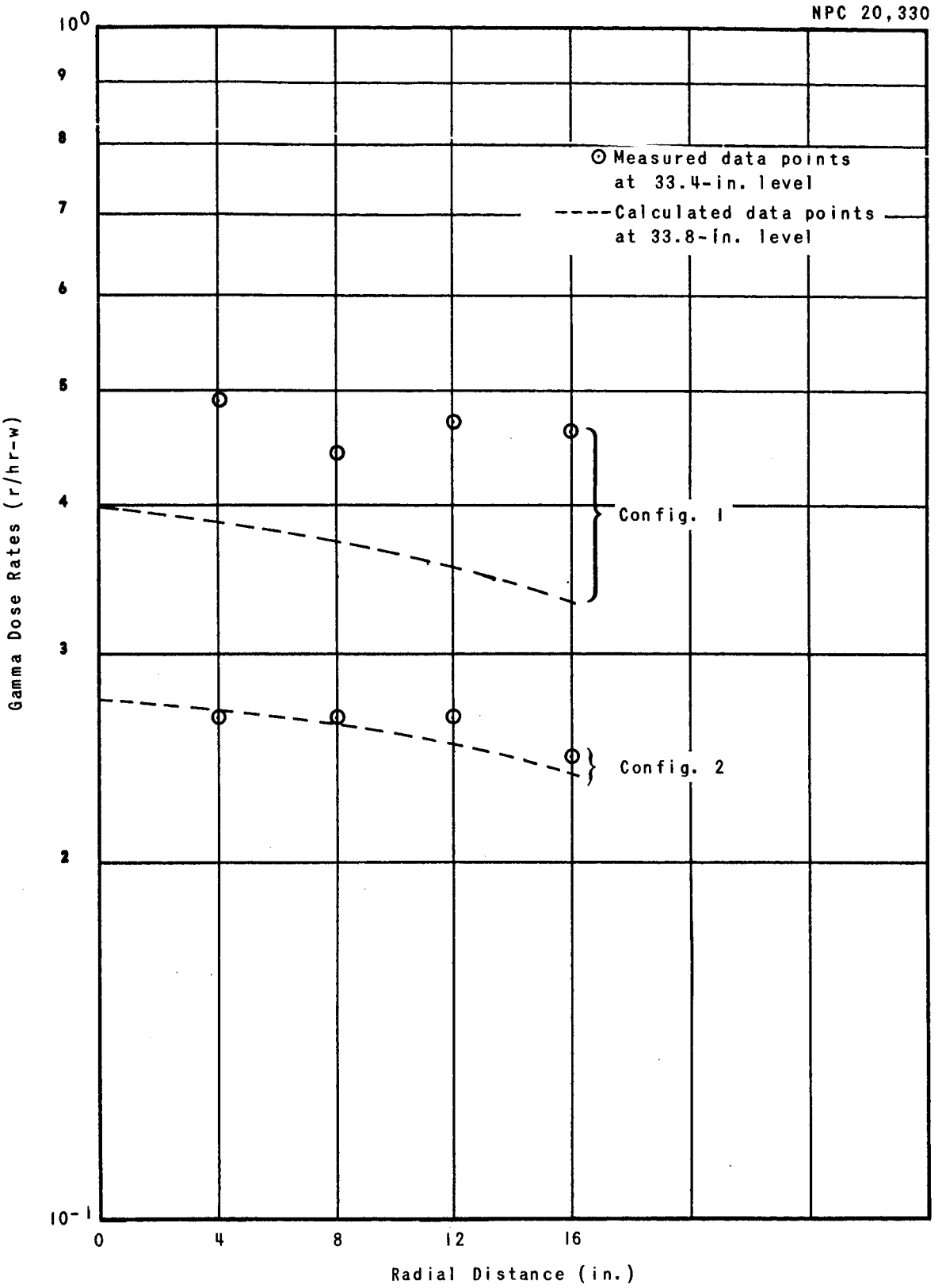

Figure 14 Total Gamma Dose Rate Distribution along Upper Radial

REFERENCES

1. Dungan, W. E., and Lewis, J. H., Nuclear Measurement Techniques for Radiation-Effects Environmental Testing. General Dynamics/Fort Worth Report FZK-9-185 (NARF-62-4T, March 1962). U

2. Peterson, D. M., Shield Penetration Programs C-17 and L-63. General Dynamics/Fort Worth Report FZK-9-170 (NARF-61-39T, December 1961). U

3. Goldstein, H., and Wilkins, J. R., Calculations of the Penetration of Gamma Rays. Nuclear Development Associates Report NYO-3075 (NDA-15C-41, June 1954). U

4. Krumbein, A. D., Summary of NDA Unclassified Results of Moments Calculations for the Penetration of Neutrons Through Various Materials. Nuclear Development Corporation of America Report NDA-92-2 (Rev.) (August 1957). U

Distribution List for Contract NAS 3-3324

National Aeronautics and Space Administration
Washington, D. C. 20546
Attention: RNN/David Novik
Attention: RNN/David J. Miller
Attention: NPO/Harold B. Finger

National Aeronautics and Space Administration
Ames Research Center
Moffet Field, California 94035
Attention: Librarian

National Aeronautics and Space Administration
Goddard Space Flight Center
Greenbelt, Maryland 20771
Attention: Librarian

National Aeronautics and Space Administration
Langley Research Center, Langley Station
Hampton, Virginia 23365
Attention: Librarian

National Aeronautics and Space Administration
Lewis Research Center
21000 Brookpark Road
Cleveland, Ohio 44135
Attention: Librarian (3)
Attention: Hugh M. Henneberry (MS 54-1)
Attention: Herman H. Ellerbrock (MS 54-1)
Attention: Donald J. Connolley (MS 54-1) (5)
Attention: AS&E Procurement Section (MS 54-1)
Attention: Norman T. Musial, Patent Counsel (MS 77-1)
Attention: I. M. Karp (MS 54-1)
Attention: Leonard Soffer (MS 100-1)
Attention: Solomon Weiss (MS 54-1)
Attention: John Liwosz (MS 54-1)

National Aeronautics and Space Administration
Manned Spacecraft Center
Houston, Texas 77001
Attention: Librarian

National Aeronautics and Space Administration
George C. Marshall Space Flight Center
Huntsville, Alabama 35812
Attention: Librarian
Attention: R. D. Shelton, Research Project Laboratory
Attention: H. L. Stern
Attention: M. O. Burrell

National Aeronautics and Space Administration
Jet Propulsion Laboratory
4800 Grove Drive
Pasadena, California 91103
Attention: Librarian

National Aeronautics and Space Administration
Space Nuclear Propulsion Office - Cleveland
Lewis Research Center
21000 Brookpark Road
Cleveland, Ohio 44135
Attention: H. S. Tuschar (MS 54-2)
Attention: J. J. Lombardo (MS 54-2)

U. S. Atomic Energy Commission
Technical Information Service Extension
Post Office Box 62
Oak Ridge, Tennessee (3)

National Aeronautics and Space Administration
Scientific and Technical Information Facility
Box 5700
Bethesda 14, Maryland (6
Attention: NASA Representative + 1 reproducible)

Los Alamos Scientific Laboratory
Post Office Box 1663
Los Alamos, New Mexico
Attention: Glen A. Graves
Attention: D. M. Peterson

General Atomic, Division of General Dynamics Corporation
Post Office Box 608
San Diego, California
Attention: J. R. Beyster

General Dynamics/Astronautics
P. O. Box 1128
San Diego, California 92112
Attention: W. K. Stromquist